Quantifying agricultural drought in tallgrass prairie region in the U.S. Southern Great Plains through analysis of a water-related vegetation index from MODIS images

Yuting Zhou[1], Xiangming Xiao[1, 2*], Geli Zhang[1], Pradeep Wagle[3], Rajen Bajgain[1], Jinwei Dong[1], Cui Jin[1], Jeffrey B. Basara[4, 5], Martha C. Anderson[6], Christopher Hain[7], Jason A. Otkin[8]

[1]Department of Microbiology and Plant Biology, and Center for Spatial Analysis, University of Oklahoma, Norman, OK 73019, USA

[2]Ministry of Education Key Laboratory of Biodiversity Science and Ecological Engineering, Institute of Biodiversity Science, Fudan University, Shanghai, 200433, China

[3]USDA-ARS Grazinglands Research Laboratory, El Reno, OK 73036, USA

[4]School of Meteorology, University of Oklahoma, Norman, OK 73019, USA

[5]Oklahoma Climate Survey, Norman, Oklahoma, USA

[6]Hydrology and Remote Sensing Laboratory, USDA Agricultural Research Service, Beltsville, Maryland, USA.

[7] NASA Marshall Space Flight Center, Earth Science Branch, Huntsville, AL, USA

[8]Cooperative Institute for Meteorological Satellite Studies, University of Wisconsin–Madison, Madison, Wisconsin, USA

*Corresponding Author：

Xiangming Xiao

Department of Microbiology and Plant Biology, Center for Spatial Analysis

University of Oklahoma

101 David L. Boren Blvd., Norman, OK 73019, USA

Phone: 405-325-8941

Email: xiangming.xiao@ou.edu

Abstract:

Severe droughts in the Southern Great Plains (SGP: Kansas, Oklahoma, and Texas) in recent years have reduced the productivity of tallgrass prairie and resulted in substantial economic losses to the beef cattle industry in this region. Understanding spatial and temporal patterns of agricultural drought in the SGP can help ranchers to develop and implement drought mitigation strategies. In this study, the Land Surface Water Index (LSWI), calculated from the Moderate Resolution Imaging Spectroradiometer (MODIS) near infrared and shortwave infrared bands, was used to assess agricultural drought in the tallgrass prairie region of the SGP during 2000-2013. The number of consecutive days with LSWI < 0 (DNLSWI) during the growing season was defined as the drought duration, which, was then used to identify and analyze frequency of summer drought and whole growing season drought (WGSD). The spatial pattern of DNLSWI was consistent with the east-to-west decreasing precipitation gradient across the SGP region. Summer drought duration as depicted by the DNLSWI in the western portion of the study area was around one and a half month. The occurrence of WGSD increased from one year in the east to up to six years in the west, demonstrating the susceptibility of the tallgrass prairie region to drought. In addition to the total amount of precipitation, its intra-annual distribution also played an important role in drought development. A comparison with other widely used national drought products, namely the Evaporative Stress Index (ESI), the Vegetation Drought Response Index (VegDRI), and the United States Drought Monitor (USDM), shows that LSWI-based drought has good agreement with ESI and USDM. Quantitative analyses indicate that LSWI-based drought agreed better with ESI in severe drought conditions than in moderate or pre-drought conditions. Severe drought periods characterized by the USDM also had low LSWI values. The areas affected by drought derived from the LSWI-based drought index were

significantly correlated with hay production. As an indicator of vegetation water stress at moderate spatial resolution (~500 m), the LSWI has the potential to show drought conditions for an individual ranch and offer guidance for drought mitigation activities and livestock production.

Keywords: Tallgrass prairie, agricultural drought, Land Surface Water Index (LSWI), Southern Great Plains (SGP)

1. Introduction

Drought is a complex natural hazard caused by a deficit in precipitation over different time periods (McKee et al. 1993). It is one of the most costly natural disasters and imposes wide-ranging impacts on the economy, environment, and society (Hayes et al. 2012; Mishra and Singh 2010). Tallgrass prairie, an important native grassland type in the Southern Great Plains (SGP: Kansas, Oklahoma, and Texas) of the United States (U.S.), is susceptible to frequent droughts (Basara et al. 2013; Christian et al. 2015; Gu et al. 2007; Gu et al. 2008; Hoerling et al. 2014; Schubert et al. 2004). Poor vegetation growth during agricultural drought reduces crop and forage production which, in turn, threatens the survival of animals and the viability of the livestock business in the SGP (Garbrecht 2015). The agricultural drought of 2011 in Texas caused more than $7.62 billion in losses, with about half of the loss attributed to reduction in livestock production (AgriLifeToday 2011; Fannin 2012; Ziolkowska 2016). Thus, it is crucial to provide information about drought characteristics (e.g., spatial distribution of different drought durations in each year) and regional drought assessment (e.g., drought severity and regional susceptibility to drought) for agricultural end users and policy-makers in the SGP to facilitate drought mitigation and adaptation decisions (Otkin et al. 2015).

Drought can be characterized from different perspectives reflecting the reduction of precipitation and/or its impacts on other factors, including runoff, streamflow, soil moisture, evapotranspiration (ET), and vegetation water stress (Fig. 1). Meteorological drought mainly focuses on deficits in precipitation. Hydrological drought depicts inadequate streamflow and/or surface and ground water levels. Agricultural drought occurs when vegetation experiences stress due to inadequate soil moisture availability, reflecting a more ecosystem point of view on the

impacts of drought. As agricultural drought develops, the plant canopy experiences a loss of vegetation water content and pigments such as chlorophyll, and eventually a loss of green leaves.

Many drought indices, based on anomalies or percentiles in relevant hydrologic variables (e.g., precipitation, soil moisture or ET), have been developed to monitor various classes of drought (Hayes 2006; Zargar et al. 2011). Among these, two meteorological drought indices, namely the Palmer Drought Severity Index (PDSI) (Palmer 1965) and the Standardized Precipitation Index (SPI) (McKee et al. 1993, 1995), are currently most widely used. These early standard meteorological drought indices (e.g., PDSI and SPI) tend to focus on precipitation deficiencies at coarse spatial resolution (i.e., the climate division level). They provide valuable information for policy makers to implement drought mitigation actions; however, these indices are usually based on sparsely located long-term meteorological stations. Hydrological drought indices often use basin-specific parameter values, making it difficult to compare among basins (Dai 2011; Mu et al. 2013). Agricultural drought indices have been developed to monitor soil water deficits and the subsequent crop failure in the drought. The Crop Moisture Index (CMI), which is related to PDSI, is able to track the agricultural drought by considering soil moisture deficit in the top 1.5 meters of soil column (Palmer 1968). The role of vegetation was not reflected in the early stages of the development of agriculture drought indices because of the complexity of different plant physiological processes and lack of data (Palmer 1965). Most agricultural drought indices use soil moisture to indicate drought and do not explicitly consider vegetation water stress (Narasimhan and Srinivasan 2005; Palmer 1965, 1968).

Satellite remote sensing is providing consistent observations of vegetation dynamics, which can be incorporated into drought monitoring over large areas at high spatial and temporal resolutions (AghaKouchak et al. 2015; Wardlow et al. 2012a). Remote sensing products such as

vegetation greenness indices, vegetation water indices, and land surface temperature have been widely used to monitor and assess drought conditions since the 1980s (Gao 1996; Hayes et al. 2012; Peters et al. 2002; Rouse Jr et al. 1974; Wan et al. 2004). At the late stage of a severe drought, plant leaves often wither and abscise, resulting in a change in leaf area index (LAI) that can be tracked by the Normalized Difference Vegetation Index (NDVI) (Fig. 1) (Cheng et al. 2006). NDVI, calculated as a normalized ratio between red and near-infrared (NIR) bands (Tucker 1979), has been incorporated into different drought products such as the Vegetation Condition Index (VCI) (Kogan 1995), Vegetation Drought Response Index (VegDRI) (Brown et al. 2008), and Vegetation Temperature Condition Index (VTCI) (Wan et al. 2004). The Enhanced Vegetation Index (EVI) is another vegetation greenness index with improved sensitivity to soil background and atmospheric condition (Huete et al. 2002). At the middle stage of agricultural drought, plant photosynthetic capacity is harmed by reduction of leaf chlorophyll content, which can be approximated by EVI as a proxy (Lawlor 2002; Medrano et al. 2002). At the early stage of agriculture drought, vegetation water stress is often characterized by the decrease of leaf water content. Water-related vegetation indices such as the Normalized Difference Water Index (NDWI) (Gao 1996) and the Land Surface Water Index (LSWI) (Xiao et al. 2004), calculated as a normalized ratio between NIR and shortwave infrared (SWIR) bands, are more sensitive to the leaf water content and water stress than are vegetation greenness indices such as NDVI and EVI (Gu et al. 2007; Gu et al. 2008; Jackson et al. 2004; Maki et al. 2004; Wagle et al. 2014). Consequently, recent studies have shown the ability of LSWI to track drought-impacted vegetation or to monitor drought (Bajgain et al. 2016; Bajgain et al. 2015; Chandrasekar et al. 2010; Wagle et al. 2015; Wagle et al. 2014).

Wagle et al. (2014) examined the seasonal dynamics of LSWI derived from the Moderate Resolution Imaging Spectroradiometer (MODIS) and the CO_2 flux data at two tallgrass prairie eddy flux tower sites during 2005-2006 in Oklahoma, and reported that LSWI < 0 during the growing season indicates drought-impacted vegetation. Another study (Bajgain et al. 2015) used LSWI to assess and track drought conditions at two tallgrass prairie sites in Oklahoma during 2000-2013 and showed that LSWI < 0 was corresponded well with moderate or severe drought categories indicated by the United States Drought Monitor (USDM) (Svoboda et al. 2002). Another follow up paper validated the LSWI-based drought algorithm for 113 Mesonet stations across Oklahoma and showed that LSWI is sensitive to rainfall variations and can be used as an indicator of drought occurrence (Bajgain et al. 2016). Based on these previous site-level findings (Bajgain et al. 2016; Bajgain et al. 2015; Wagle et al. 2014), we hypothesize that the LSWI-based drought algorithm can be applied to assess the drought dynamics of tallgrass prairie at the regional scale such as in the SGP.

The specific objectives of this study are (1) to apply the LSWI-based drought algorithm in the tallgrass prairie of the SGP during 2000-2013; (2) to analyze the impacts of precipitation distribution on different drought patterns; and (3) to compare the LSWI-based drought map with other U.S. national drought products such as the Evaporative Stress Index (ESI) (Anderson et al. 2011; Anderson et al. 2007; Otkin et al. 2013), VegDRI (Brown et al. 2008), and USDM (Svoboda et al. 2002), during normal, summer drought, and growing season drought years.

2. Materials and methods

2.1 Study area

This study focuses on the SGP region in the U.S., specifically including Kansas (KS), Oklahoma (OK), and Texas (TX) (Fig. 2). These three states are known for extensive ranching and farming. The mean annual precipitation (MAP) shows a decreasing gradient from east (1400 mm) to west (200-400 mm) across the region (http://www.prism.oregonstate.edu/normals/). Precipitation is highly variable both inter- and intra-annually (Christian et al. 2015; Flanagan et al. 2017; Weaver et al. 2016). Maximum temperatures in summer are usually associated with low atmospheric humidity and strong winds, which in turn produce high rates of soil moisture depletion through ET, the main reason for summer drought (Dong et al. 2011). Soil types are mainly sandy and clay with small surface slopes (Carter 1994). Shortgrass prairies are distributed in the arid and semiarid western part of the SGP, while tallgrasses prairies are primarily located in the sub-humid eastern part of the region (Carter 1994).

2.2 Data

2.2.1 MODIS-based LSWI and NDVI

The SGP is covered by six MODIS tiles (Fig. 2). The 8-day composite MODIS Surface Reflectance product at a 500-m spatial resolution (MOD09A1) (Vermote and Vermeulen 1999) was used to calculate LSWI and NDVI at 500 m. MOD09A1 includes seven-bands: blue (459-479 nm), green (545-565 nm), red (620-670 nm), two near infrared (NIR_1: 841-876 nm; NIR_2: 1230-1250 nm), and two shortwave infrared ($SWIR_1$: 1628-1652 nm, $SWIR_2$: 2105-2155 nm) bands at a 500-m spatial resolution. MOD09A1 also includes quality control flags for consideration of various image artifacts (e.g., clouds and cloud shadow). For each 8-day composite image, LSWI (Xiao et al. 2002a, b) and NDVI (Tucker 1979) were calculated using surface reflectance (ρ) from MODIS red, near infrared (NIR_1) and shortwave infrared bands ($SWIR_1$) as:

$$LSWI = \frac{\rho_{nir} - \rho_{swir}}{\rho_{nir} + \rho_{swir}} \quad (1)$$

$$NDVI = \frac{\rho_{nir} - \rho_{red}}{\rho_{nir} + \rho_{red}} \quad (2)$$

2.2.2 MODIS Land Surface Temperature (LST) data

The MODIS 8-day Land Surface Temperature (LST) product (MOD11A2) at a 1-km spatial resolution from 2000 to 2013 was used to depict the nighttime LST (LST_{night}) (Wan and Dozier 1996) and define the thermal growing season. Detailed descriptions of MOD11A2 can be found at https://lpdaac.usgs.gov/dataset_discovery/modis/modis_products_table/mod11a2. The LST data were resampled from 1-km to 500-m spatial resolution using nearest neighbor interpolation. To evaluate the effects of resampling of LST on data processing, we compared the start date and end date of LST > 5^{o}C (SOD and EOD) before and after resampling based on one tile of the MODIS (h10v05) LST data in 2012 (Fig. S1). The two figures in each group look very similar to each other. The means of SOD and EOD were close in the corresponding group (Table. S1).

Fig. S1. Images for the start date and end date of LST > 5^{o}C (SOD and EOD) before and after resampling. (a) SOD before resampling; (b) SOD after resampling; (c) EOD before resampling; (d) EOD after resampling.

Table. S1 The comparison of the start date and end date of LST > 5^{o}C (SOD and EOD) before and after resampling.

2.2.3 MODIS Land Cover Type data

The MODIS Land Cover Type product (MCD12Q1) was used to generate the grassland mask (Friedl et al. 2002) and then to define the tallgrass prairie layer. The IGBP (International

Geosphere-Biosphere Program) classification scheme was used, which includes a grassland class (https://lpdaac.usgs.gov/dataset_discovery/modis/modis_products_table/mcd12q1).

2.2.4 Precipitation data

Precipitation data were downloaded from PRISM Climate Group, Oregon State University (http://prism.oregonstate.edu). The time series of precipitation datasets are modeled using climatologically-aided interpolation, which uses the long-term average pattern (i.e., the 30-year normals) as first-guess of the spatial pattern of climatic conditions for a given month or day. Monthly precipitation data for 2000-2013 were used to generate summer precipitation (June-August, JJA) and annual precipitation.

Precipitation data measured by automated weather stations covering Oklahoma were also included to evaluate the LSWI-based drought at site level. The dataset was acquired from a previous LSWI-based drought related study in Oklahoma (Bajgain et al. 2016). The precipitation anomalies were compared against LSWI anomalies at 113 Mesonet stations across Oklahoma for the drought years.

2.2.5 Forage production data

Forage production, especially for hay, is affected by drought as most of the hay producing fields rely on rainfall. Hay production data from the United States Department of Agriculture - National Agricultural Statistics Service (https://www.nass.usda.gov/Quick_Stats/) were used to evaluate the LSWI-based drought depictions in each state included in the study. A simple linear regression model was used to examine the relationships between drought affected area and hay production for each state.

2.3 Algorithms for mapping agricultural drought

Based on findings from our previous studies (Bajgain et al. 2016; Bajgain et al. 2015; Wagle et al. 2014) that the LSWI can assess the impact of drought on tallgrass prairie vegetation at individual sites, this study aims to expand its use to identify both summer drought and whole growing season drought (WGSD) conditions at the regional scale (SGP). Fig. 3 illustrates the steps in the drought identification algorithm as applied to MODIS time series data for a given year. Nighttime LST data from the entire year were first used to determine the temperature-defined growing season, which is the time between the start and end dates for consecutive three 8-day periods with nighttime LST > 5^{o}C (Morison and Morecroft 2008; Zhang et al. 2015; Zhou et al. 2016). Second, the drop of LSWI below zero during summer (JJA) was used to indicate severe agricultural drought in summer (Bajgain et al. 2015). Third, the summer drought duration maps were generated by counting the number of days with LSWI < 0 (these days do not need to be consecutive) in JJA (DNLSWI). Years with all LSWI values less than zero during the LST-defined plant growing season were defined as WGSD years (Fig. 3).

As the LSWI-based drought algorithm was originally developed for the tallgrass prairie, we focused on tallgrass prairie area in this study. The tallgrass prairie map was generated as the study area mask based on the MODIS land cover maps (MCD12Q1) for 2001-2013 and LSWI data. The grassland layer from MCD12Q1 for 2001 was used as a close approximation of 2000 since the MCD12Q1 dataset starts from 2001. Using these time series, the number of years that each pixel classified as grassland was computed, as well as the annual maximum value of LSWI ($LSWI_{max}$) during the LST-based growing season. To exclude sparse vegetation areas, the tallgrass mask was generated by selecting those pixels that meet two criteria over 14 years: (1) the number of years as grassland is 7 or more (50% or higher) and (2) the number of years with

$LSWI_{max} > 0$ is 7 or more (50% or higher) (Fig. 2 inset). This tallgrass prairie mask was then used to conduct the analyses of drought duration described later in the manuscript (Fig. S2).

Fig. S2. Data processing workflow for LSWI-based drought assessment algorithm.

2.4 Agricultural drought dynamics and comparison with other drought products

Annual agricultural drought maps were created to show the evolution of agricultural drought over the study period. Each drought map includes both summer and WGSD conditions. The drought maps for three consecutive years (2010, 2011, and 2012) were selected to represent three different drought conditions (normal, WGSD, and summer drought). WGSD and summer drought years were identified from annual and summer precipitation anomalies (Fig. S3), respectively, based on the fourteen-year mean (2000-2013). A mean summer drought duration map was generated showing the average drought duration for 2000-2013. The occurrence of WGSD map shows the frequency of WGSD during the study area from 2000 to 2013. These two summary maps indicate the spatial pattern of agricultural drought in the tallgrass region in the SGP.

Fig. S3. Annual, early spring, and summer precipitation deviation from the mean.

Three U.S. national drought products, namely ESI, VegDRI, and USDM, were also compared with the LSWI-based drought product to characterize different drought conditions. The ESI (Anderson et al. 2013; Anderson et al. 2011; Anderson et al. 2007) quantifies temporal anomalies in the ratio of actual to potential ET using thermal infrared remote sensing observations and the Atmosphere-Land Exchange Inverse (ALEXI) surface energy balance model. It has been used to estimate the moisture stress of plants, as well as associated yield impacts (Anderson et al. 2016a; Anderson et al. 2015; Anderson et al. 2016b). VegDRI is a new

'hybrid' index that integrates satellite-based observations of vegetation conditions, climate-based drought index data, and biophysical characteristics of the environment, including PDSI, SPI, and NDVI, to depict drought-related vegetation stress (Brown et al. 2008; Tadesse et al. 2015; Wardlow et al. 2012b). The USDM is a composite drought index which incorporates climatic, hydrologic, and soil data along with professional inputs in order to provide weekly maps of drought conditions (Svoboda et al. 2002).

A direct comparison between the LSWI-based drought with ESI, VegDRI, and USDM is difficult due to their differences in temporal scales and spatial resolutions. ESI data are provided at weekly time steps composited over a period of 1-3 months. The VegDRI and USDM are also created weekly. In this study, we used 3-month ESI composites ending on the last week of August to compare with LSWI-based drought duration. The VegDRI and USDM for the last week of August were used in the comparison. The comparison was done for the period 2010-2012, which represent three different drought conditions (normal, WGSD, and summer drought).

2.5 The relationship between precipitation and LSWI-based drought duration

Because agricultural drought is triggered in part by a precipitation deficit, it is worthwhile to investigate the relationship between precipitation and LSWI-based drought duration. Summer drought duration from LSWI-based drought maps and cumulative summer rainfall (JJA) from PRISM data for 2010-2012 were extracted and analyzed. The relationships between summer drought duration and summer rainfall were analyzed and the pattern of cumulative summer rainfall in different drought condition years are also presented. The site-level precipitation data from the Oklahoma Mesonet were also used to evaluate the LSWI-based drought. The spatial patterns of WGSD and annual precipitation deviation from the mean in 2011 (WGSD year)

demonstrate the effects of annual precipitation on the WGSD. The relationship between WGSD affected area and the annual precipitation anomaly was also investigated.

3. Results

3.1 LSWI-based drought maps and comparison with ESI, VegDRI, and USDM

The tallgrass prairie in the SGP was affected by frequent droughts during the study period (Fig. S4) and the drought duration was consistent with the decreasing precipitation gradient from east to west in most years (Fig. 2). Some areas experienced a short duration of summer drought even in a normal rainfall year (e.g., 2010, Fig. 4a). Central SGP experienced a long period of summer drought in 2012 (indicated by dark red color) (Fig. 4i). 2011 was the most severe WGSD year in OK and TX (indicated by black color), with more than half of the tallgrass prairie areas affected (Fig. 4e). For KS, 2002 was the most severe WGSD year (Fig. S4c).

Fig. S4. Drought dynamics in the SGP for 2000-2013.

Fig. 4 shows ESI, VegDRI, and USDM summer drought depictions for 2010-2012, and compares with spatial patterns in the LSWI-based drought duration. The LSWI-based drought map, ESI, and VegDRI provided more detailed drought information than did USDM because of their higher spatial resolution and number of drought categories. The LSWI-based drought map showed a short period of drought occurrence in the western SGP even in a normal year (2010) (Fig. 4a), while summer ESI indicated wet or near normal conditions for most of the areas (Fig. 4b) and VegDRI showed scattered pre-drought and unusually moist with big non-photosynthetically-active vegetation area (out of season category in the figure) (Fig.4c). In 2011, all drought products identified extended/severe drought conditions in the central SGP (Fig. 4e-h). The four indices were different in their depictions of the 2012 drought conditions (Fig. 4i-l), with

LSWI-based drought, ESI, and USDM showing extensive and severe drought for KS and OK, while VegDRI mostly indicating pre-drought to moderate drought. The increasing drought gradient from east to west in the LSWI-based drought map was not apparent in other drought indices except for VegDRI in 2011 (Fig. 4g).

In general, the patterns of LSWI-based summer drought maps are similar with those in the ESI and USDM for most of the areas (Fig. 4). However, the VegDRI tends to show less intense drought conditions than other drought products for the same year. One possible reason is that VegDRI uses long-term climate variables such as 36-week SPI which responds more slowly than LSWI and ESI. Similar findings were identified in a study by Otkin et al (Otkin et al. 2016).

LSWI, ESI, and VegDRI over the SGP tallgrass prairie regions were also compared quantitatively. Fig. 5 compares ESI values from the 3-month composite ending at the last week of August with LSWI-based drought duration for 2012, which is the period with severe summer drought. A clear trend of increasing ESI stress severity is identified with increasing length of drought conditions as identified by the LSWI. The dynamic range of ESI decreased along with the increasing summer drought duration (Fig. 5), indicating that LSWI-based drought and ESI agree better for severe drought than moderate or pre-drought conditions. The relationship between LSWI and VegDRI showed a stronger trend than did the relationship between NDVI and VegDRI (Fig. S5).

Fig. S5. LSWI and NDVI vs. VegDRI for the last week of August in 2012. Only pixels classified as tallgrass prairie were plotted.

LSWI values are compared to the USDM drought severity classifications from the last week of August in 2012 in Fig. 6. Most areas depicted as experiencing severe drought according

to the USDM (D3 and D4) also have very low LSWI values (Fig. 6b inset) such as western KS and southern TX (Fig. 6a). As two key indicators in the USDM are usually available only at the climate division scale, the USDM does not show much variability in drought severity within a climate division. In contrast, LSWI shows large heterogeneity at the sub-climate division scale due to the relative high spatial resolution of the remotely sensed inputs.

3.2 LSWI-based drought duration patterns in the SGP

Fig. 7 shows the dynamics of summer drought duration diagnosed by LSWI in three states (KS, OK, and TX) for 2000-2013. The summer drought pattern was highly variable among years in all three states. TX was affected by summer drought more often than KS and OK. 2012 was the most severe summer drought year in OK, with relatively small area affected by short periods of drought and large areas affected by longer periods of drought (Fig. 7b). The frequent occurrence of summer drought indicates the susceptibility of the SGP to agricultural drought. Fig. 8 shows the areas affected by WGSD across the region for 2000-2013. The pattern of WGSD in OK and TX were similar with 2011 as the most severe WGSD year, while it was 2002 in the case of KS. In the most severe WGSD years, the area affected by WGSD was more than double of the mean value.

Fig. 9 shows the mean of summer drought duration, standard deviation of summer drought duration, and frequency of the occurrence of WGSD for 2000-2013. As expected, both summer drought duration and occurrence of WGSD increased from east to west, along the gradient of decreasing precipitation. Mean summer drought duration can be as long as one and a half months (six 8-day periods) (Fig. 9a) and WGSD occurred in six years (Fig. 9c) in the west of the study area. The variability in summer drought duration was largest in the central part (Fig. 9b).

3.3 Relationship between LSWI-based drought duration and precipitation

To quantify the contribution of precipitation deficits to drought development, we examined the relationship between precipitation and drought duration during the summer period and the entire year. The variation of the summer drought duration (indicated by error bar) was equally large for all precipitation ranges (Fig. 10), suggesting that summer precipitation is not the only factor determining summer drought duration. The cumulative summer precipitation (indicated by the relative frequency of precipitation) in 2010 (Fig. 10a) was slightly higher than in 2012 (Fig. 10c), whereas the summer drought duration was quite different, with much longer summer drought duration in 2012. More than 60% percent of the pixels had less than 100 mm of cumulative summer precipitation in 2011 and long periods of summer drought. (Fig. 10b).

The LSWI anomalies were strongly correlated with summer precipitation anomalies (r^2 = 0.64) for the drought years (2006, 2011, and 2012) over 113 Mesonet stations across Oklahoma (Fig. 11a). The increasing summer precipitation anomalies resulted in bigger magnitude of anomalies in LSWI at most Mesonet stations. The drought intensity indicated by USDM was not highly correlated with the summer precipitation anomalies (Fig. 11b).

Areas affected by WGSD increased from north to south in the SGP in 2011 (Fig. 12a). This trend correlates well with the annual precipitation deviation to the mean in 2011 (Fig. 12b). The mean value of the annual precipitation deficit in 2011 was 300 mm (Fig. 12b inset and Fig. S6) which is about one third of the long term mean annual precipitation (Fig. 2). Precipitation deviation from the mean (annual anomaly in 2011) in central and southern TX was as high as 400 mm or more. The increasing temperature gradient from north to south might also have exacerbated drought in the southern region.

Fig. S6. Frequency distribution of the annual precipitation deviation from the mean in 2011.

To investigate the relationship between the WGSD affected area and annual precipitation anomalies, we plotted the ratio of WGSD affected areas to total state area against annual precipitation anomalies for all three states during 2000-2013 (Fig. 13). Overall, larger anomalies in annual precipitation resulted in larger areas affected by WGSD. The point in the upper right corner is associated with large annual precipitation anomaly in 2011, demonstrating the severity of 2011 Texas drought.

3.4 Validation of LSWI-based drought against forage production

Fig. 14 show the relationships between areas affected by drought (summer drought and WGSD) and hay production in each state during 2000-2013. The hay production showed a significant negative relationship with areas affected by drought. The lowest hay production year was 2011 in KS and TX and 2012 in OK. This is consistent with our results that 2011 and 2012 were the most severe drought years.

4. Discussion

4.1 Comparison of the LSWI-based drought algorithm with other drought products

The LSWI-based drought algorithm uses LSWI values less than zero during the growing season to identify agricultural drought conditions based on the findings of previous studies at individual sites (Bajgain et al. 2015; Wagle et al. 2014). The SWIR band in LSWI is more sensitive to the canopy water content (high absorption by liquid water) than the red band used in NDVI (Gu et al. 2007; Gu et al. 2008; Jackson et al. 2004). Thus, the LSWI-based algorithm complements well with other NDVI-based drought products, as they together assess the impacts of drought on vegetation canopy from a loss of water to a loss of green leaves (Fig. 1).

Furthermore, previous study showed that LSWI provided an earlier signal of declining soil moisture than did NDVI and EVI (Bajgain et al. 2015) which might be useful for drought early warning. This study expanded the LSWI-based drought algorithm to include three conditions: no drought, summer drought, and WGSD, and then applied the algorithm at the regional scale (tallgrass prairie region in the SGP) to report agricultural drought conditions.

Similar spatial patterns of LSWI-based summer drought maps with ESI and USDM (Fig.4), and strong relationships of low LSWI values with ESI (Fig.5) and USDM categories (Fig. 6) during the severe drought indicate that LSWI can be used as a complementary drought index. The significant negative relationship between drought affected areas and hay yield further validated the reliability of the LSWI-based drought mapping. Using LSWI along with other commonly used vegetation indices such as NDVI and EVI can help improve the performance of current drought products. The LSWI-based drought algorithm completely depends on MODIS data and is easy to apply. It could be a complementary method for assessing agricultural drought in the tallgrass prairie at the regional scale with a spatial resolution of 500 m.

4.2 Importance of precipitation amount and distribution in the year

As expected, our results show that precipitation is a major factor for the occurrence of severe agricultural drought in tallgrass prairie since the regional agricultural drought pattern (Fig. 9a and c) was highly correlated with the decreasing precipitation gradient from east to west. Central SGP had long summer drought durations and large standard deviations (Fig. 9a and b) because of large summer precipitation variations (Fig. S7). The orthogonal nature of the temperature and precipitation gradients (east-west oriented precipitation gradient and north-south oriented temperature gradient) (Basara et al. 2013) could also generate this pattern in the central

part of the SGP where the relative importance of temperature and precipitation varies in different years.

Fig. S7. Standard deviation of summer precipitation.

The total amount of precipitation in a year is important for vegetation. Large annual precipitation deficits in 2011 (Fig. 12) caused the occurrence of extensive WGSD in the SGP (Fig. 4e). The temporal distribution of precipitation is also equally important. The cumulative summer precipitation in 2012 was only a little bit lower than 2010 (Fig. 10), however, the drought condition in 2012 was much more severe (Fig. 4). The precipitation in early spring (March) was well distributed in 2012 (Fig. 15a). The ample precipitation in March 2012 (Fig. S3f and Fig. 15a) increased soil moisture and facilitated vegetation growth in spring (the anomaly of high NDVI is presented in Fig. S8). Summer rainfall was much less than the enhanced ET demand from abundant green vegetation, resulted in rapid depletion of soil moisture and severe summer drought in 2012. This result indicated that it was the joint control of precipitation and vegetation that generated the severe summer drought in 2012. It suggests the important role of vegetation itself for the occurrence of agricultural drought in addition to total amount of precipitation. This phenomenon has been reported by other studies (Otkin et al. 2013; Otkin et al. 2014; Otkin et al. 2016) and referred as "flash drought" in which vegetation health rapidly deteriorates because the plants quickly exhaust soil moisture. Thus, LSWI-based drought does not only reflect precipitation anomalies to the historical mean as SPI does but is also sensitive to abnormal precipitation distribution in the year.

Fig. S8. NDVI anomaly in early growing season of 2012 (March-May) relative to the baseline of 2000 - 2011. The inset shows the distribution of area percent of NDVI anomalies.

4.3 Future work and challenges

The LSWI-based drought algorithm, which only uses MODIS data as input, is easy to apply and has a higher spatial resolution (~500 m) than current operational versions of ESI, VegDRI, and USDM. Like most visible and thermal remote sensing algorithms, the LSWI-based drought algorithm has limitations during cloudy days when the land surface is not visible to the satellite sensor (Jensen 2009). Combinations of multiple satellite sensors and development of an appropriate gap-filling algorithm are needed to create a continuous dataset (Jin et al. 2013), thereby reducing the effect of bad observations (e.g., cloud cover). Another concern is the threshold values used in the algorithm. We used LSWI < 0 during the growing season as the indicator of severe agricultural drought in tallgrass prairie based on the findings of site level studies (Bajgain et al. 2015; Wagle et al. 2014). The LSWI threshold for other land cover types and regions might be different, which needs to be further explored. The identification of agricultural drought in sparse vegetation area (e.g. arid region) using LSWI is challenging as soil background can contribute more to the satellite observations and reduce LSWI values. In these cases, the lower threshold of relative change of LSWI values might be better. Also LSWI is related to vegetation water content, it is not able to depict drought during the non-growing season. Additional studies are needed to develop a LSWI-based drought severity scheme based on plant phenology and anomalies. In this study, we evaluated and reported agricultural drought in terms of severe drought duration in the summer and entire growing season, and drought severity at specific times was not included. Future studies need to compare the LSWI-based drought severity scheme at specific times (Bajgain et al. 2016; Bajgain et al. 2015) with ESI, USDM, and other drought products. Human and natural disturbances (grazing, mowing, and burning etc.)

could also affect LSWI, which needs to be incorporated using land use and land management data.

The relationship between precipitation and drought needs to be further investigated as other studies indicated that high temperature can also contribute to the quick onset of drought in the SGP (Basara et al. 2013; Hoerling et al. 2014; Otkin et al. 2013; Otkin et al. 2016). The importance of vegetation in agricultural drought assessment needs to be emphasized in the future as precipitation does not always provide accurate drought assessment without considering the high ET demand by vegetation and available soil moisture in summer. Plant health can deteriorate rapidly during the summer through rapid loss of water because of their high ET. The ESI, an indicator of ET anomaly, is a good indicator to reflect the role of vegetation in agricultural drought development (Anderson et al. 2011; Anderson et al. 2007; Otkin et al. 2016). The importance of vegetation in drought development also emphasizes the necessity of investigating drought from the ecosystem perspective (AghaKouchak et al. 2015).

The duration of summer drought, summer drought variation, and number of years with WGSD present the pattern of agricultural drought in tallgrass prairie in the SGP (Fig. 9). The LSWI-based drought algorithm can be used to assess the vulnerability to agricultural drought, and it has the potential to use for several applications such as vegetation production assessment, water demand/supply analysis, and bird migration and breeding (Brown and Brown 2014; Goddard et al. 2003; Wilhite 2005). The agricultural drought of tallgrass prairie in the SGP reduces hay production (Fig. 14), an important feed source for beef cattle production, especially in winter and early spring, which can threaten the beef cattle industry. A follow-up study will use the LSWI-based drought product to investigate the impacts of different drought types (e.g., summer drought and WGSD) and spatial patterns on hay and beef cattle production in the SGP.

5. Conclusion

Based on the findings of previous studies about the ability of LSWI to track drought-impacted vegetation in tallgrass prairie, this study expanded and applied a LSWI-based drought algorithm to map agricultural drought of tallgrass prairie in the SGP. The results are comparable to other widely used drought products (ESI, VegDRI, and USDM) in normal, WGSD, and summer drought years. The frequent occurrence of summer drought and WGSD indicates the susceptibility of the SGP to agricultural drought. The spatial pattern of drought duration was highly correlated with the decreasing precipitation gradient from east to west. TX was affected by summer drought more often than KS and OK. In the most severe WGSD years, the area affected by WGSD was more than double of the mean value. LSWI-based drought depictions are sensitive to both precipitation anomalies from the historical mean and abnormal seasonal precipitation distributions. The importance of vegetation in drought assessment needs to be emphasized in future drought studies. Incorporating LSWI other than NDVI into other drought products can help improve their performance. The LSWI-based drought algorithm, completely depending on MODIS data and with a spatial resolution of 500 m, can be a complement for other drought products for assessment of agricultural drought in the tallgrass prairie region. Future studies need to explore LSWI thresholds to identify agricultural drought and develop LSWI-based drought severity schemes for other land cover types.

Acknowledgements

This study was supported in part by research grants from the USDA National Institute of Food and Agriculture (grant number 2013-69002-23146 and 2016-68002-24967), the National Science Foundation (NSF) EPSCoR (IIA-1301789), and NOAA Climate Office's Sectoral Applications Research Program (SARP) grant NA130AR431012. We would like to acknowledge

Dr. Jianyang Xia, Dr. Zheng Shi, and Junyi Liang for their suggestions in the early stage of the manuscript and Hayden Mahan and Nicholas Cejda for English editing of the manuscript. We would like to thank the anonymous reviewers for their constructive comments and suggestions on the earlier version of the manuscript.

References

AghaKouchak, A., Farahmand, A., Melton, F., Teixeira, J., Anderson, M., Wardlow, B., & Hain, C. (2015). Remote sensing of drought: Progress, challenges and opportunities. *Reviews of Geophysics, 53*, 452-480

AgriLifeToday (2011). Texas Agricultural Drought Losses Reach Record $5.2 Billion

Anderson, M.C., Hain, C., Otkin, J., Zhan, X., Mo, K., Svoboda, M., Wardlow, B., & Pimstein, A. (2013). An intercomparison of drought indicators based on thermal remote sensing and NLDAS-2 simulations with US Drought Monitor classifications. *Journal of Hydrometeorology, 14*, 1035-1056

Anderson, M.C., Hain, C., Wardlow, B., Pimstein, A., Mecikalski, J.R., & Kustas, W.P. (2011). Evaluation of drought indices based on thermal remote sensing of evapotranspiration over the continental United States. *Journal of Climate, 24*, 2025-2044

Anderson, M.C., Hain, C.R., Frantisek, J., Trnka, M., Hlavinka, P., Dulaney, W., Otkin, J.A., Johnson, D., & Gao, F. (2016a). Relationships between the evaporative stress index and winter wheat and spring barley yield anomalies in the Czech Republic. *Climate Research, 70*, 215-230

Anderson, M.C., Norman, J.M., Mecikalski, J.R., Otkin, J.A., & Kustas, W.P. (2007). A climatological study of evapotranspiration and moisture stress across the continental United States based on thermal remote sensing: 2. Surface moisture climatology. *Journal of Geophysical Research: Atmospheres (1984–2012), 112*

Anderson, M.C., Zolin, C.A., Hain, C.R., Semmens, K., Yilmaz, M.T., & Gao, F. (2015). Comparison of satellite-derived LAI and precipitation anomalies over Brazil with a thermal infrared-based Evaporative Stress Index for 2003–2013. *Journal of Hydrology, 526*, 287-302

Anderson, M.C., Zolin, C.A., Sentelhas, P.C., Hain, C.R., Semmens, K., Yilmaz, M.T., Gao, F., Otkin, J.A., & Tetrault, R. (2016b). The Evaporative Stress Index as an indicator of agricultural drought in Brazil: An assessment based on crop yield impacts. *Remote Sensing of Environment, 174*, 82-99

Bajgain, R., Xiao, X., Basara, J., Wagle, P., Zhou, Y., Zhang, Y., & Mahan, H. (2016). Assessing agricultural drought in summer over Oklahoma Mesonet sites using the water-

related vegetation index from MODIS. *International Journal of Biometeorology, 10.1007/s00484-016-1218-8*, 1-14

Bajgain, R., Xiao, X., Wagle, P., Basara, J., & Zhou, Y. (2015). Sensitivity analysis of vegetation indices to drought over two tallgrass prairie sites. *ISPRS Journal of Photogrammetry and Remote Sensing, 108*, 151-160

Basara, J.B., Maybourn, J.N., Peirano, C.M., Tate, J.E., Brown, P.J., Hoey, J.D., & Smith, B.R. (2013). Drought and associated impacts in the Great Plains of the United States—A review. *International Journal of Geosciences, 4*, 72

Brown, C.R., & Brown, M.B. (2014). Breeding time in a migratory songbird is predicted by drought severity and group size. *Ecology, 95*, 2736-2744

Brown, J.F., Wardlow, B.D., Tadesse, T., Hayes, M.J., & Reed, B.C. (2008). The Vegetation Drought Response Index (VegDRI): A new integrated approach for monitoring drought stress in vegetation. *GIScience & Remote Sensing, 45*, 16-46

Carter, M.R. (1994). *Conservation tillage in temperate agroecosystems*. Lewis Publishers Inc.

Chandrasekar, K., Sesha Sai, M., Roy, P., & Dwevedi, R. (2010). Land Surface Water Index (LSWI) response to rainfall and NDVI using the MODIS Vegetation Index product. *International Journal of Remote Sensing, 31*, 3987-4005

Cheng, Y.-B., Zarco-Tejada, P.J., Riaño, D., Rueda, C.A., & Ustin, S.L. (2006). Estimating vegetation water content with hyperspectral data for different canopy scenarios: Relationships between AVIRIS and MODIS indexes. *Remote Sensing of Environment, 105*, 354-366

Christian, J., Christian, K., & Basara, J.B. (2015). Drought and pluvial dipole events within the great plains of the United States. *Journal of Applied Meteorology and Climatology, 54*, 1886-1898

Dai, A. (2011). Drought under global warming: a review. *Wiley Interdisciplinary Reviews: Climate Change, 2*, 45-65

Dong, X., Xi, B., Kennedy, A., Feng, Z., Entin, J.K., Houser, P.R., Schiffer, R.A., L'Ecuyer, T., Olson, W.S., Hsu, K.-l., Liu, W.T., Lin, B., Deng, Y., & Jiang, T. (2011). Investigation of the 2006 drought and 2007 flood extremes at the Southern Great Plains through an integrative analysis of observations. *Journal of Geophysical Research: Atmospheres, 116*, n/a-n/a

Fannin, B. (2012). Updated 2011 texas agricultural drought losses total $7.62 billion. *Southwest Farm Press, Retrieved from http://search.proquest.com/docview/929437522?accountid=12964*

Flanagan, P.X., Basara, J.B., & Xiao, X. (2017). Long-term analysis of the asynchronicity between temperature and precipitation maxima in the United States Great Plains. *International Journal of Climatology*

Friedl, M.A., McIver, D.K., Hodges, J.C., Zhang, X., Muchoney, D., Strahler, A.H., Woodcock, C.E., Gopal, S., Schneider, A., & Cooper, A. (2002). Global land cover mapping from MODIS: algorithms and early results. *Remote Sensing of Environment, 83*, 287-302

Gao, B.-c. (1996). NDWI—A normalized difference water index for remote sensing of vegetation liquid water from space. *Remote Sensing of Environment, 58*, 257-266

Garbrecht, J.D. (2015). Soil water signature of the 2005-2006 drought under tallgrass prairie at Fort Reno, Oklahoma. In, *Proceedings of the Oklahoma Academy of Science* (pp. 37-44)

Goddard, S., Harms, S.K., Reichenbach, S.E., Tadesse, T., & Waltman, W.J. (2003). Geospatial decision support for drought risk management. *Communications of the ACM, 46*, 35-37

Gu, Y., Brown, J.F., Verdin, J.P., & Wardlow, B. (2007). A five‐year analysis of MODIS NDVI and NDWI for grassland drought assessment over the central Great Plains of the United States. *Geophysical Research Letters, 34*

Gu, Y., Hunt, E., Wardlow, B., Basara, J.B., Brown, J.F., & Verdin, J.P. (2008). Evaluation of MODIS NDVI and NDWI for vegetation drought monitoring using Oklahoma Mesonet soil moisture data. *Geophysical Research Letters, 35*

Hayes, M., Svoboda, M., Wardlow, B., Anderson, M., & Kogan, F. (2012). Drought monitoring: Historical and current perspectives. *Remote sensing of drought*, 1-19

Hayes, M.J. (2006). *Drought indices*. Wiley Online Library

Hoerling, M., Eischeid, J., Kumar, A., Leung, R., Mariotti, A., Mo, K., Schubert, S., & Seager, R. (2014). Causes and predictability of the 2012 Great Plains drought. *Bulletin of the American Meteorological Society, 95*, 269-282

Huete, A., Didan, K., Miura, T., Rodriguez, E.P., Gao, X., & Ferreira, L.G. (2002). Overview of the radiometric and biophysical performance of the MODIS vegetation indices. *Remote Sensing of Environment, 83*, 195-213

Jackson, T.J., Chen, D., Cosh, M., Li, F., Anderson, M., Walthall, C., Doriaswamy, P., & Hunt, E.R. (2004). Vegetation water content mapping using Landsat data derived normalized difference water index for corn and soybeans. *Remote Sensing of Environment, 92*, 475-482

Jensen, J.R. (2009). *Remote Sensing of the Environment: An Earth Resource Perspective*. Pearson Education India

Jin, C., Xiao, X., Merbold, L., Arneth, A., Veenendaal, E., & Kutsch, W.L. (2013). Phenology and gross primary production of two dominant savanna woodland ecosystems in Southern Africa. *Remote Sensing of Environment, 135*, 189-201

Kogan, F. (1995). Application of vegetation index and brightness temperature for drought detection. *Advances in Space Research, 15*, 91-100

Lawlor, D.W. (2002). Limitation to Photosynthesis in Water‐stressed Leaves: Stomata vs. Metabolism and the Role of ATP. *Annals of Botany, 89*, 871-885

Maki, M., Ishiahra, M., & Tamura, M. (2004). Estimation of leaf water status to monitor the risk of forest fires by using remotely sensed data. *Remote Sensing of Environment, 90*, 441-450

McKee, T.B., Doesken, N.J., & Kleist, J. (1993). The relationship of drought frequency and duration to time scales. In, *Proceedings of the 8th Conference on Applied Climatology* (pp. 179-183): American Meteorological Society Boston, MA

McKee, T.B., Doesken, N.J., & Kleist, J. (1995). Drought monitoring with multiple time scales. In, *Ninth Conference on Applied Climatology. American Meteorological Society, Boston*

Medrano, H., Escalona, J., Bota, J., Gulias, J., & Flexas, J. (2002). Regulation of photosynthesis of C3 plants in response to progressive drought: stomatal conductance as a reference parameter. *Annals of Botany, 89*, 895-905

Mishra, A.K., & Singh, V.P. (2010). A review of drought concepts. *Journal of Hydrology, 391*, 202-216

Morison, J.I., & Morecroft, M.D. (2008). *Plant growth and climate change*. John Wiley & Sons

Mu, Q., Zhao, M., Kimball, J.S., McDowell, N.G., & Running, S.W. (2013). A remotely sensed global terrestrial drought severity index. *Bulletin of the American Meteorological Society, 94*, 83-98

Narasimhan, B., & Srinivasan, R. (2005). Development and evaluation of Soil Moisture Deficit Index (SMDI) and Evapotranspiration Deficit Index (ETDI) for agricultural drought monitoring. *Agricultural and Forest Meteorology, 133*, 69-88

Otkin, J.A., Anderson, M.C., Hain, C., Mladenova, I.E., Basara, J.B., & Svoboda, M. (2013). Examining Rapid Onset Drought Development Using the Thermal Infrared–Based Evaporative Stress Index. *Journal of Hydrometeorology, 14*, 1057-1074

Otkin, J.A., Anderson, M.C., Hain, C., & Svoboda, M. (2014). Examining the relationship between drought development and rapid changes in the evaporative stress index. *Journal of Hydrometeorology, 15*, 938-956

Otkin, J.A., Anderson, M.C., Hain, C., Svoboda, M., Johnson, D., Mueller, R., Tadesse, T., Wardlow, B., & Brown, J. (2016). Assessing the evolution of soil moisture and vegetation conditions during the 2012 United States flash drought. *Agricultural and Forest Meteorology, 218-219*, 230-242

Otkin, J.A., Shafer, M., Svoboda, M., Wardlow, B., Anderson, M.C., Hain, C., & Basara, J. (2015). Facilitating the Use of Drought Early Warning Information through Interactions with Agricultural Stakeholders. *Bulletin of the American Meteorological Society*

Palmer, W.C. (1965). *Meteorological drought*. US Department of Commerce, Weather Bureau Washington, DC, USA

Palmer, W.C. (1968). Keeping track of crop moisture conditions, nationwide: The new crop moisture index

Peters, A.J., Walter-Shea, E.A., Ji, L., Vina, A., Hayes, M., & Svoboda, M.D. (2002). Drought monitoring with NDVI-based standardized vegetation index. *Photogrammetric engineering and remote sensing, 68*, 71-75

Rouse Jr, J.W., Haas, R., Schell, J., & Deering, D. (1974). Monitoring vegetation systems in the Great Plains with ERTS. *NASA special publication, 351*, 309

Schubert, S.D., Suarez, M.J., Pegion, P.J., Koster, R.D., & Bacmeister, J.T. (2004). On the cause of the 1930s Dust Bowl. *Science, 303*, 1855-1859

Svoboda, M., LeComte, D., Hayes, M., Heim, R., Gleason, K., Angel, J., Rippey, B., Tinker, R., Palecki, M., & Stooksbury, D. (2002). The drought monitor. *Bulletin of the American Meteorological Society, 83*, 1181-1190

Tadesse, T., Wardlow, B.D., Brown, J.F., Svoboda, M.D., Hayes, M.J., Fuchs, B., & Gutzmer, D. (2015). Assessing the Vegetation Condition Impacts of the 2011 Drought across the U.S. Southern Great Plains Using the Vegetation Drought Response Index (VegDRI). *Journal of Applied Meteorology and Climatology, 54*, 153-169

Tucker, C.J. (1979). Red and photographic infrared linear combinations for monitoring vegetation. *Remote Sensing of Environment, 8*, 127-150

Vermote, E., & Vermeulen, A. (1999). Atmospheric correction algorithm: spectral reflectances (MOD09). *ATBD version, 4*

Wagle, P., Xiao, X., & Suyker, A.E. (2015). Estimation and analysis of gross primary production of soybean under various management practices and drought conditions. *ISPRS Journal of Photogrammetry and Remote Sensing, 99*, 70-83

Wagle, P., Xiao, X., Torn, M.S., Cook, D.R., Matamala, R., Fischer, M.L., Jin, C., Dong, J., & Biradar, C. (2014). Sensitivity of vegetation indices and gross primary production of tallgrass prairie to severe drought. *Remote Sensing of Environment, 152*, 1-14

Wan, Z., & Dozier, J. (1996). A generalized split-window algorithm for retrieving land-surface temperature from space. *Geoscience and Remote Sensing, IEEE Transactions on, 34*, 892-905

Wan, Z., Wang, P., & Li, X. (2004). Using MODIS Land Surface Temperature and Normalized Difference Vegetation Index products for monitoring drought in the southern Great Plains, USA. *International Journal of Remote Sensing, 25*, 61-72

Wardlow, B.D., Anderson, M.C., & Verdin, J.P. (2012a). *Remote sensing of drought: Innovative monitoring approaches*. CRC Press

Wardlow, B.D., Tadesse, T., Brown, J.F., Callahan, K., Swain, S., & Hunt, E. (2012b). The Vegetation Drought Response Index (VegDRI): An integration of satellite, climate, and biophysical data

Weaver, S., Baxter, S., & Harnos, K. (2016). Regional Changes in the Interannual Variability of U.S. Warm Season Precipitation. *Journal of Climate, 29*, 5157-5173

Wilhite, D.A. (2005). *Drought and water crises: science, technology, and management issues*. CRC Press

Xiao, X., Boles, S., Frolking, S., Salas, W., Moore Iii, B., Li, C., He, L., & Zhao, R. (2002a). Landscape-scale characterization of cropland in China using Vegetation and Landsat TM images. *International Journal of Remote Sensing, 23*, 3579-3594

Xiao, X., Boles, S., Frolking, S., Salas, W., Moore Iii, B., Li, C., He, L., & Zhao, R. (2002b). Observation of flooding and rice transplanting of paddy rice fields at the site to landscape

scales in China using VEGETATION sensor data. *International Journal of Remote Sensing, 23*, 3009-3022

Xiao, X., Hollinger, D., Aber, J., Goltz, M., Davidson, E.A., Zhang, Q., & Moore Iii, B. (2004). Satellite-based modeling of gross primary production in an evergreen needleleaf forest. *Remote Sensing of Environment, 89*, 519-534

Zargar, A., Sadiq, R., Naser, B., & Khan, F.I. (2011). A review of drought indices. *Environmental Reviews, 19*, 333-349

Zhang, G., Xiao, X., Dong, J., Kou, W., Jin, C., Qin, Y., Zhou, Y., Wang, J., Menarguez, M.A., & Biradar, C. (2015). Mapping paddy rice planting areas through time series analysis of MODIS land surface temperature and vegetation index data. *ISPRS Journal of Photogrammetry and Remote Sensing, 106*, 157-171

Zhou, Y., Xiao, X., Qin, Y., Dong, J., Zhang, G., Kou, W., Jin, C., Wang, J., & Li, X. (2016). Mapping paddy rice planting area in rice-wetland coexistent areas through analysis of Landsat 8 OLI and MODIS images. *International Journal of Applied Earth Observation and Geoinformation, 46*, 1-12

Ziolkowska, J. (2016). Socio-Economic Implications of Drought in the Agricultural Sector and the State Economy. *Economies, 4*, 19

Figures

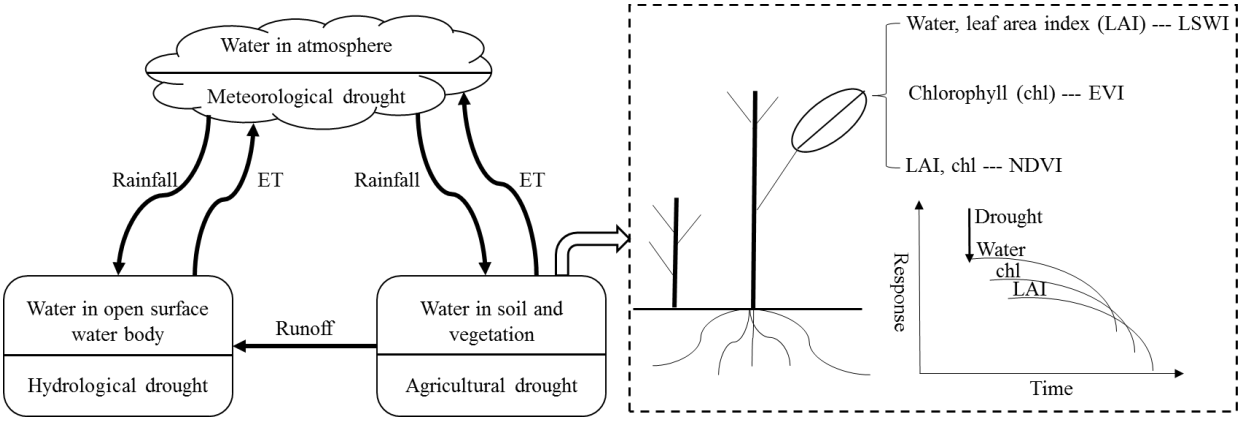

Fig. 1. Different timescales of drought, highlighting observables of vegetation water stress expressed as remote sensing proxies. Only the primary factors affecting the remotely sensed vegetation indices are listed.

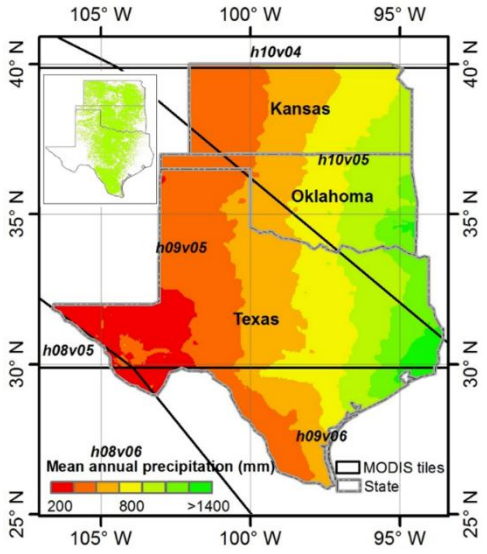

Fig. 2. Location of the Southern Great Plains (SGP) study area and the coverage of the tallgrass prairie (in the inset). MODIS tile boundaries are indicated as dark lines. The base map shows the 30 year (1981-2010) mean annual precipitation over the region.

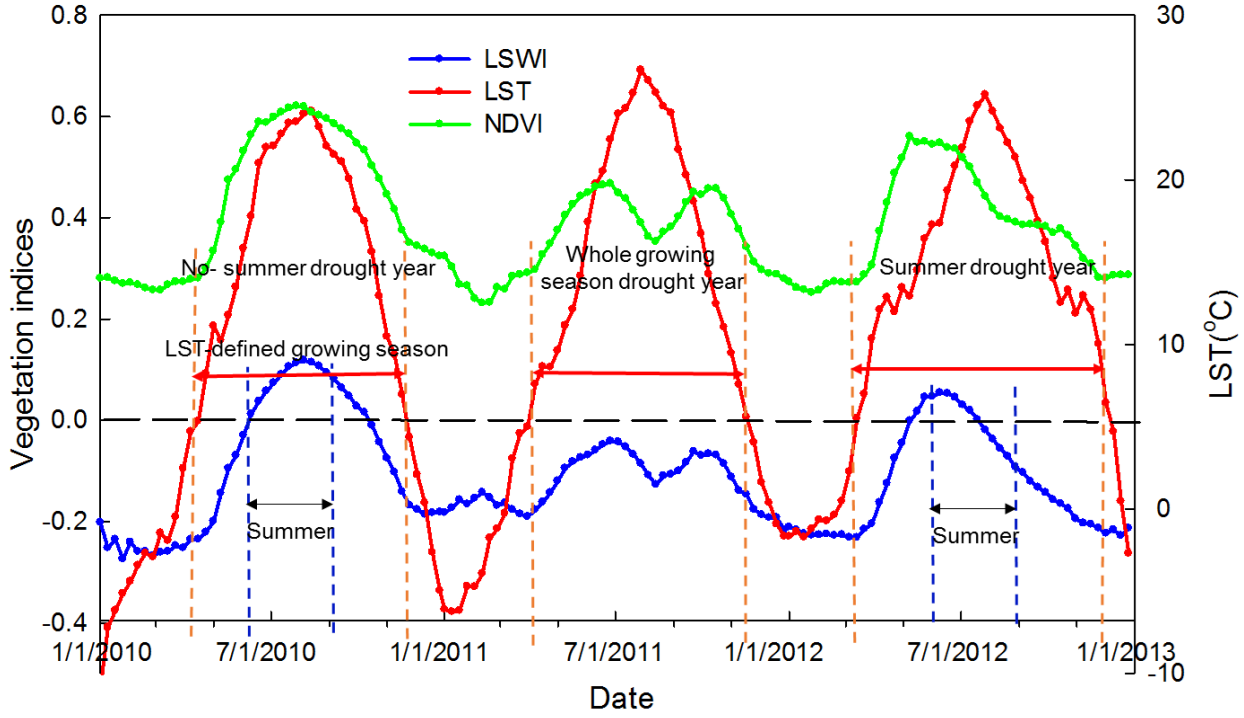

Fig. 3. A schematic diagraph of the seasonal dynamics of LST, LSWI, and NDVI during drought and non-drought years for a sample data point is located at 36.556481°N, -98.317713°W. The LST-defined growing season is depicted for the duration of nighttime LST > 5 °C.

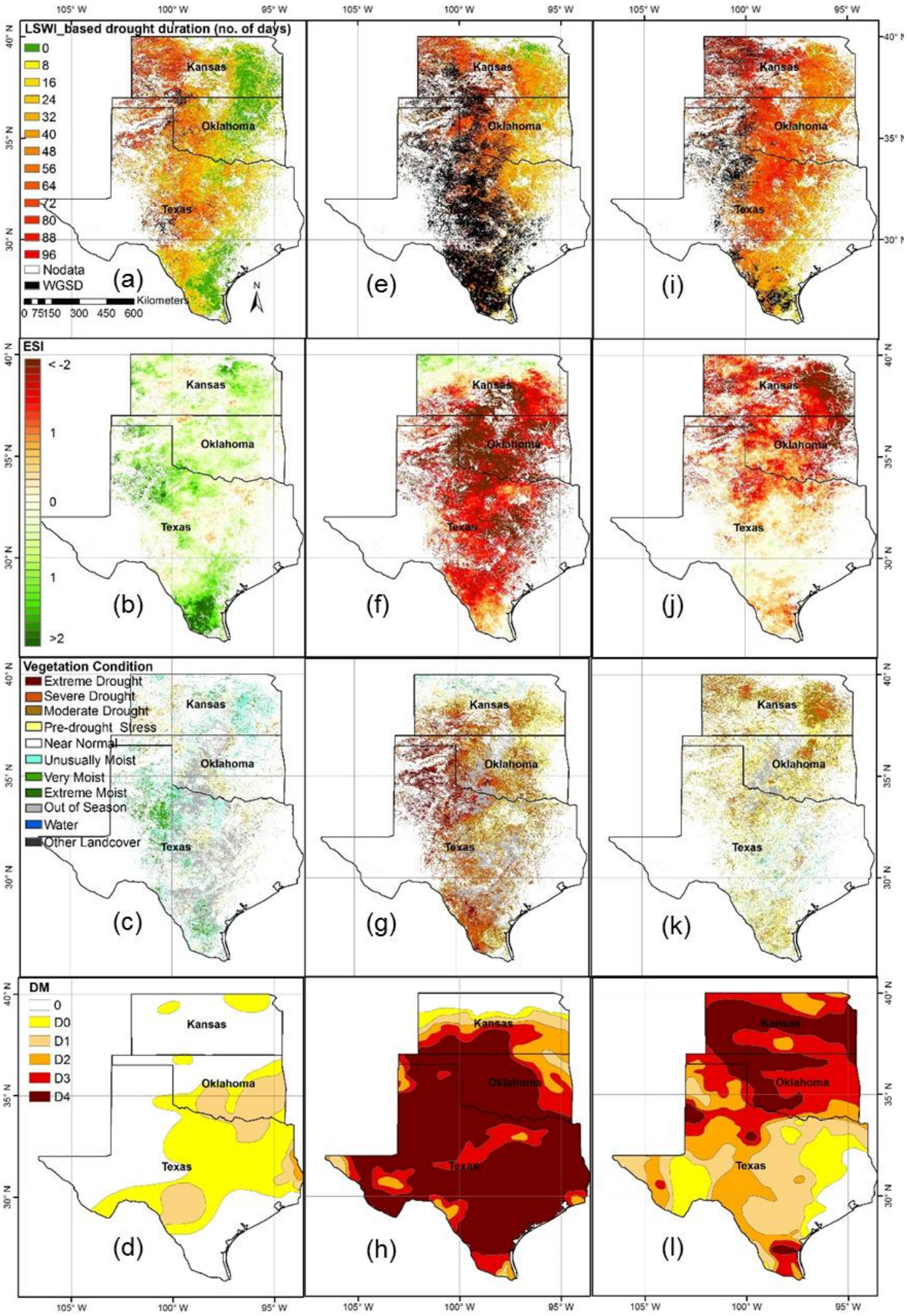
LSWI_based drought duration (no. of days)
0
8
16
24
32
40
48
56
64
72
80
88
96
Nodata
WGSD
Kilometers
0 75150 300 450 600
N
(a)
(e)
(i)
ESI
< -2
1
0
1
>2
(b)
(f)
(j)
Vegetation Condition
Extreme Drought
Severe Drought
Moderate Drought
Pre-drought Stress
Near Normal
Unusually Moist
Very Moist
Extreme Moist
Out of Season
Water
Other Landcover
(c)
(g)
(k)
DM
0
D0
D1
D2
D3
D4
(d)
(h)
(l)
Kansas
Oklahoma
Texas
105° W
100° W
95° W
40° N
35° N
30° N

Fig. 4. Comparison of LSWI-based drought duration with ESI, VegDRI, and USDM in normal, WGSD, and summer drought years. (a) Summer drought duration and WGSD in 2010, (b) Summer ESI in 2010, (c) Summer VegDRI in 2010, (d) USDM 20100831, (e) Summer drought duration and WGSD in 2011 (f) Summer ESI in 2011, (g) Summer VegDRI in 2011, (h) USDM 20110830, (i) Summer drought duration and WGSD in 2012, (j) Summer ESI in 2012, (k) Summer VegDRI in 2012, (l) USDM 20120828.

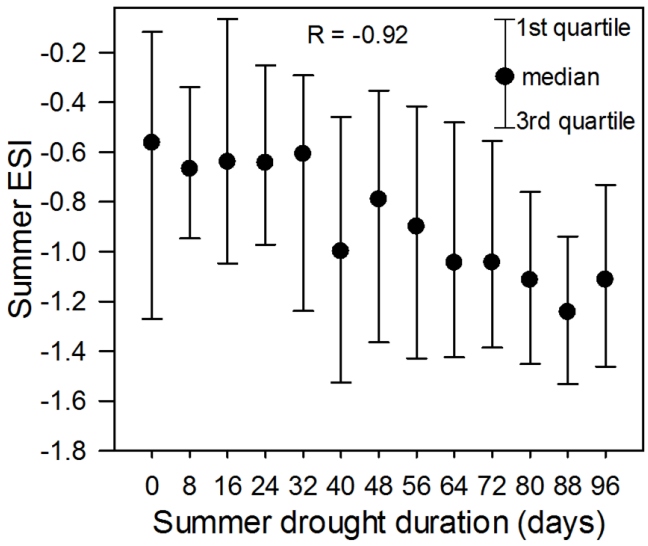

Fig. 5. LSWI-based summer drought duration vs. 3-month composite ESI (JJA) in 2012.

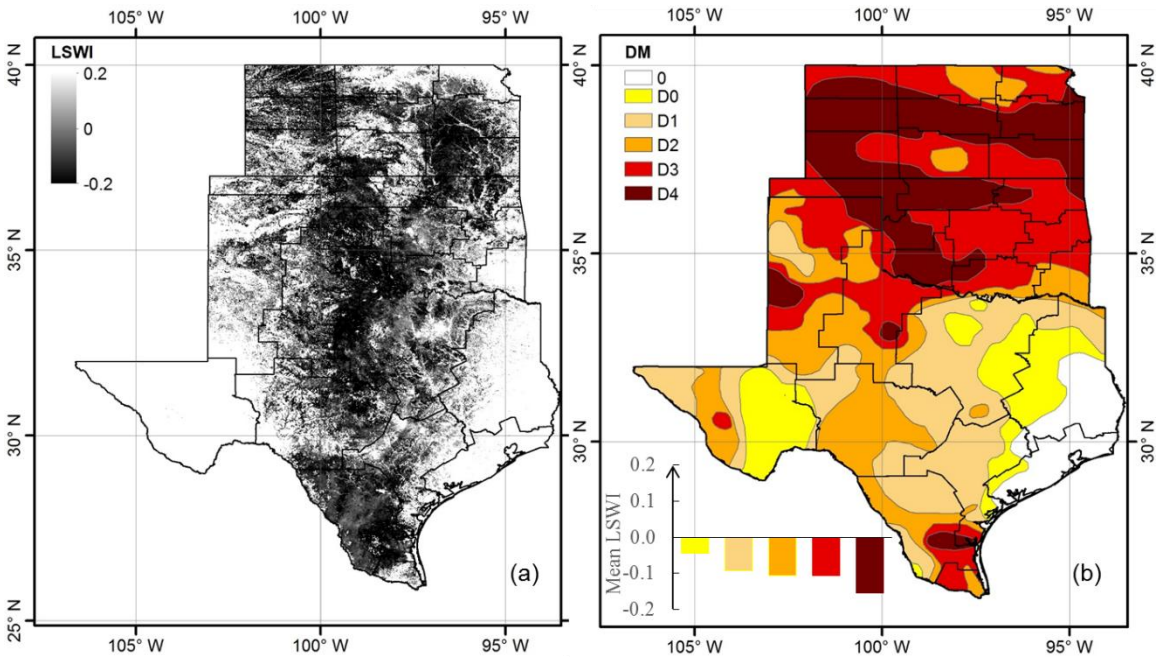

Fig. 6. LSWI vs. USDM for the last week of August in 2012. The climate division boundaries are indicated by black polygons. Only pixels classified as tallgrass prairie were plotted. The inset in (b) showed the mean LSWI values in each category (D0, D1, D2, D3, and D4).

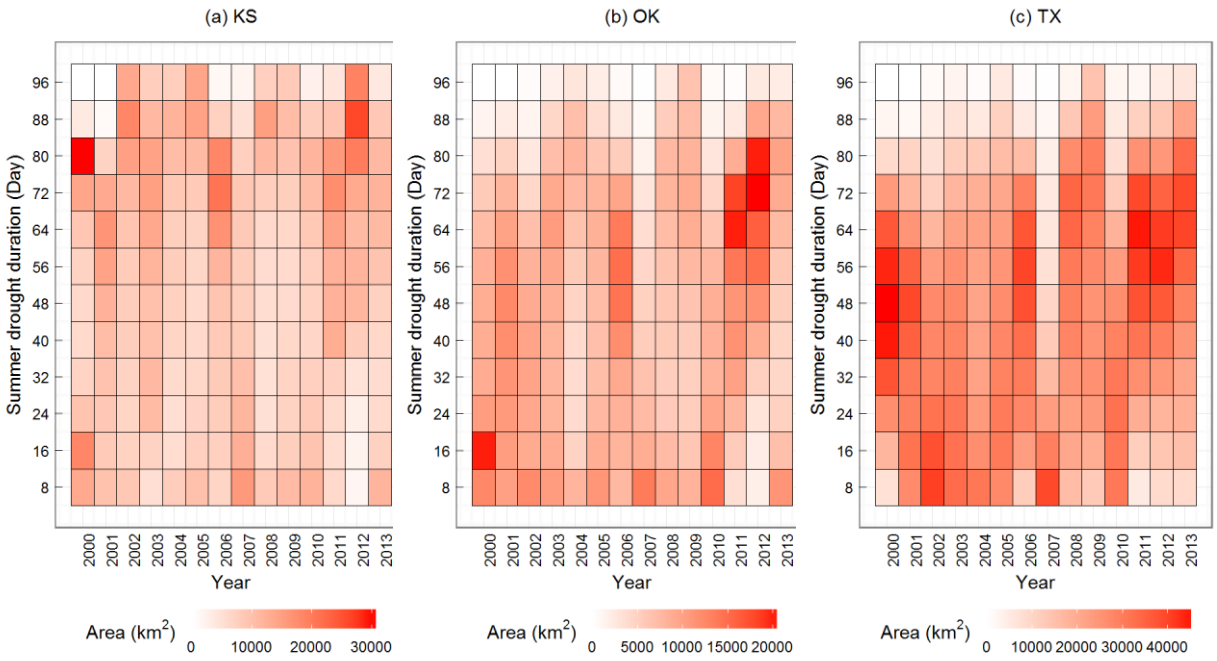

Fig. 7. Annual summer drought dynamics in three states (KS, OK, and TX) of the SGP for 2000-2013.

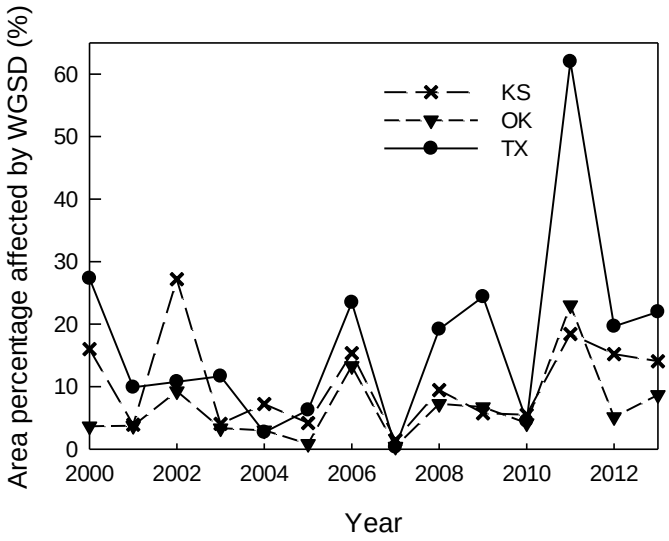

Fig. 8. Areal percentage of the total tallgrass prairie area affected by the whole growing season drought (WGSD) in three states (KS, OK, and TX) of the SGP for 2000-2013.

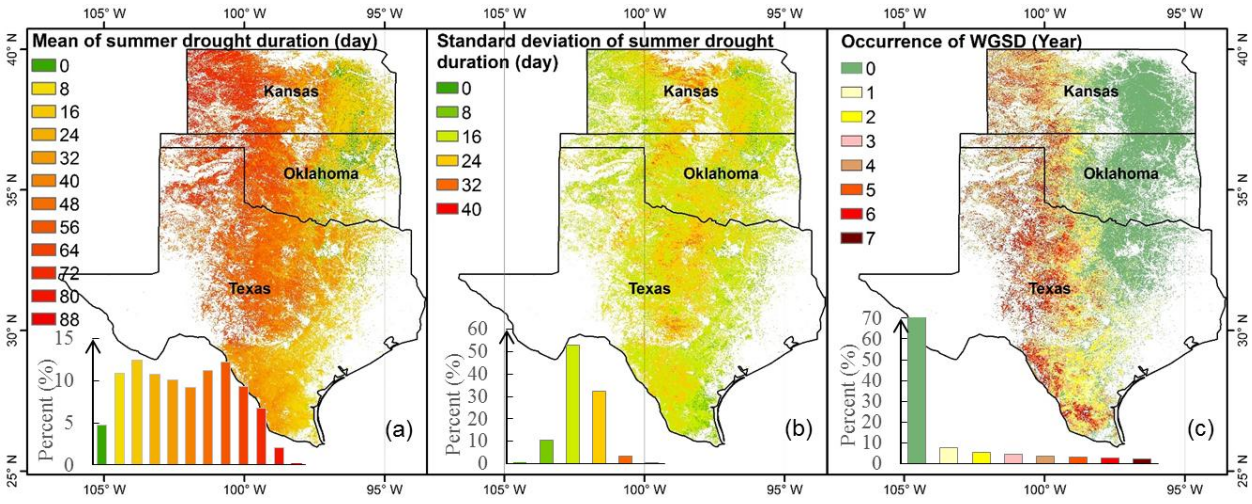

Fig. 9. Summer drought and WGSD patterns in the SGP for 2000-2013. (a) Mean of summer drought duration for 2000-2013, (b) Standard deviation of summer drought duration, (c) Occurrence of WGSD for 2000-2013. The insert panel shows the frequency distribution of values.

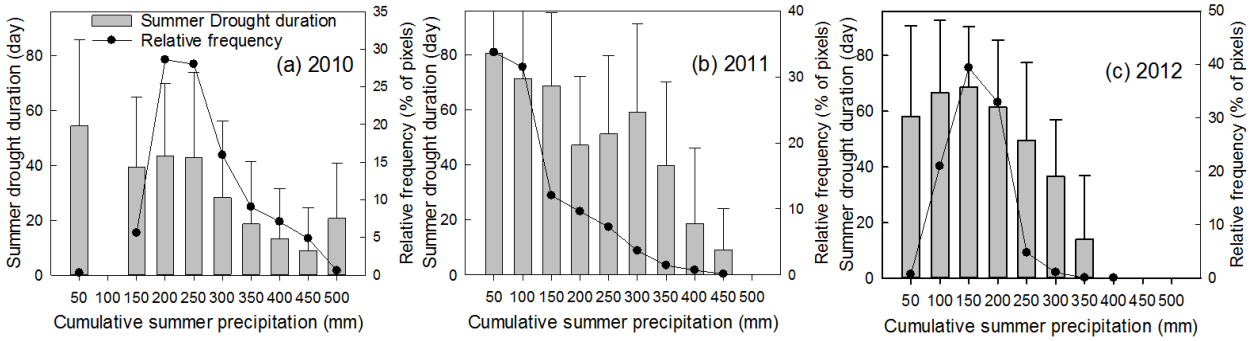

Fig. 10. LSWI-based summer drought duration vs. summer precipitation in (a) 2010, (b) 2011, and (c) 2012. Relative frequency in the legend indicates the ratio of pixels with certain summer precipitation to the total pixels.

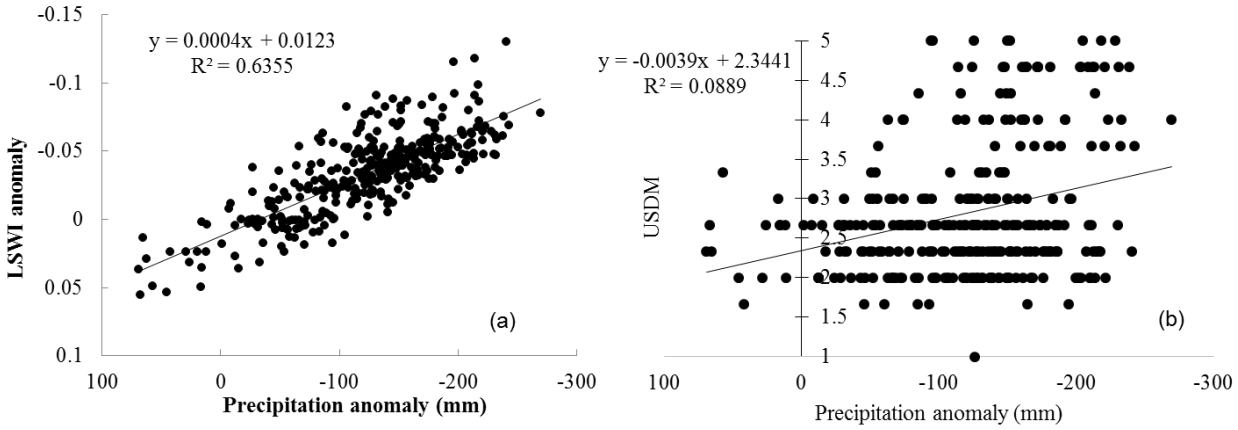

Fig. 11. Comparison of summer precipitation anomalies and LSWI anomalies (a) and USDM (b) in drought years (2006, 2011, and 2012) at 113 Mesonet stations across OK. The USDM drought intensity classes 0, D0, D1, D2, D3, and D4 are set to 0, 1, 2, 3, 4, and 5, respectively.

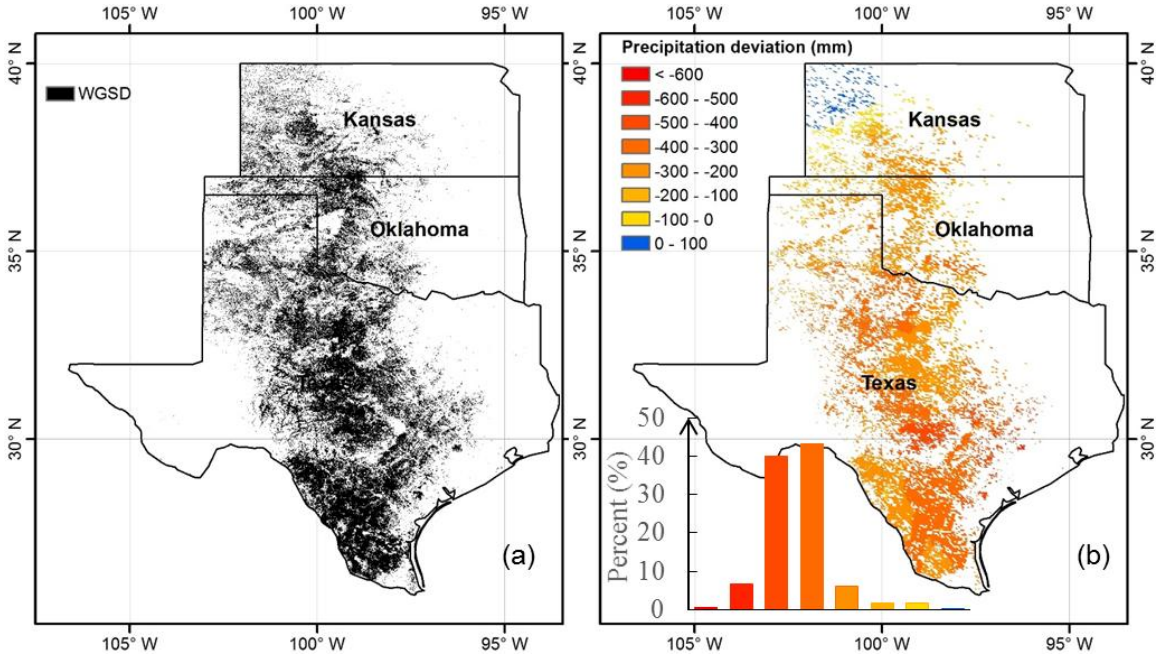

Fig. 12. WGSD vs. annual precipitation in 2011. (a) Distribution of WGSD in 2011, (b) Annual precipitation deviation from the mean (annual anomaly in 2011). The inset in (b) shows the frequency distribution of precipitation deviation.

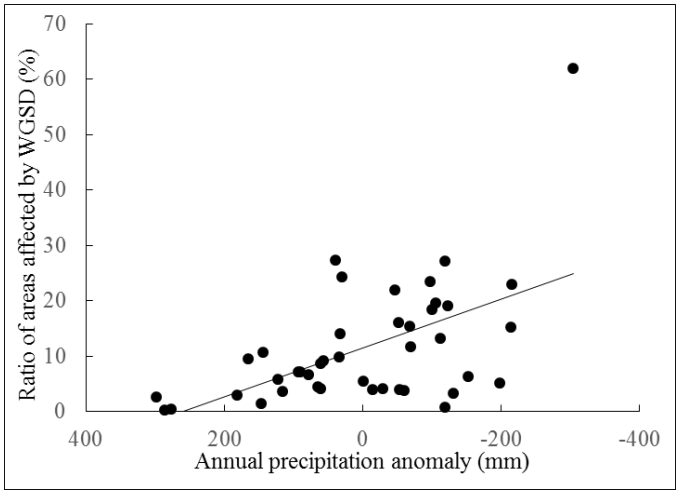

Fig. 13. Relationship between the WGSD affected area and annual precipitation anomaly.

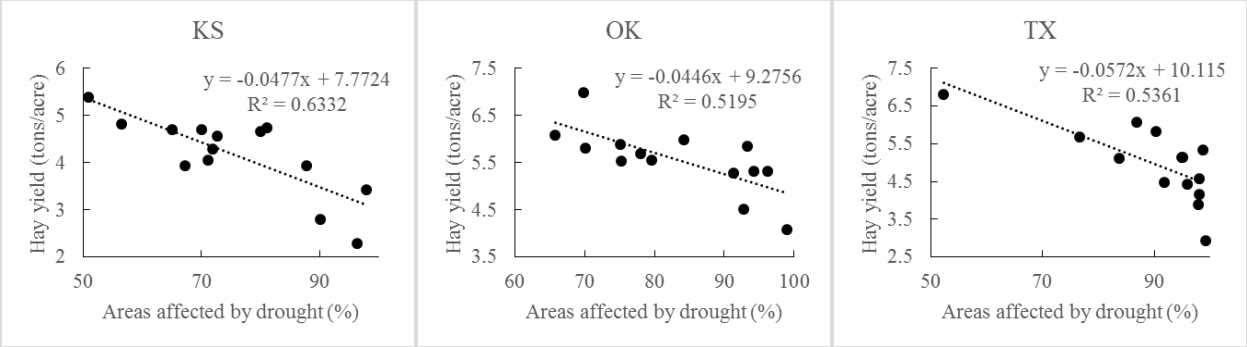

Fig. 14. Relationship between areas affected by drought and hay production in each state.

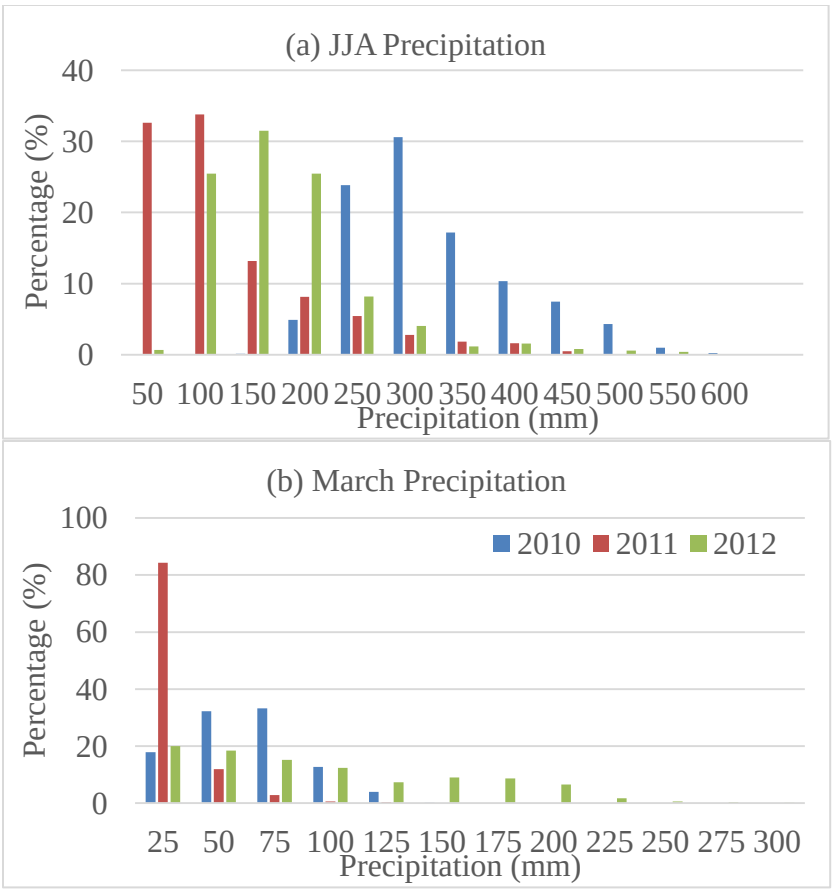

Fig. 15. Precipitation distribution in early (March) and peak growing season (June-August) according to rainfall events (%) with different rainfall sizes (25 mm rainfall bin size in the graph).